Construction and Building Materials 232 (2020) 117265

Contents lists available at ScienceDirect

Construction and Building Materials

journal homepage: www.elsevier.com/locate/conbuildmat

Waste-derived glass-ceramics fired in nitrogen: Stabilization and functionalization

Patricia Rabelo Monich [a], Acacio Rincón Romero [a], Daniele Desideri [b], Enrico Bernardo [a,*]

[a] Dipartimento di Ingegneria Industriale, Università degli Studi di Padova, Via Marzolo 9, Padova 35131, Italy
[b] Dipartimento di Ingegneria Industriale, Università degli Studi di Padova, Via Gradenigo 6/A, Padova 35131, Italy

HIGHLIGHTS

- Highly porous glass-ceramics obtained by direct foaming of alkali activated glass slurries.
- Control of phase evolution by adjustment of firing temperature and atmosphere.
- Firing in N_2 promoted the stabilization of pollutants and novel functionalities.
- Porous glass-ceramics fired at 1000 °C exhibited high dielectric permittivity.
- Firing at 800 °C led to electrically conductive foams for electromagnetic shielding.

ARTICLE INFO

Article history:
Received 10 June 2019
Received in revised form 3 October 2019
Accepted 12 October 2019

Keywords:
Gel casting
Alkali activation
Glass ceramics
Foams
Electromagnetic shielding

ABSTRACT

In a circular economy perspective, waste-derived materials are attractive once the adopted manufacturing technology combines low costs, absolute stabilization of pollutants and interesting functionalities of the product. This paper deals with the enhancement of chemical stability and functionalities of highly porous glass-ceramic foams, from vitreous residues the plasma processing of municipal solid waste ('Plasmastone'), by firing in nitrogen, at 800–1000 °C. Before firing, the processing relied on alkali activation of glass suspensions, followed by intensive mechanical stirring. Previous experiments had demonstrated that the stabilization of pollutants could be achieved only by mixing Plasmastone with 30 wt% recycled boro-alumino-silicate glass, in samples fired in air. The change in the atmosphere had a significant impact on the Fe^{2+}/Fe^{3+} balance, leading to a different phase assemblage, in turn causing the stabilization of pollutants even operating with more common recycled soda-lime glass. The new phase assemblage also promoted functionalities such as electrical conductivity, relative permittivity and electromagnetic shielding effectiveness.

© 2019 The Author(s). Published by Elsevier Ltd. This is an open access article under the CC BY-NC-ND license (http://creativecommons.org/licenses/by-nc-nd/4.0/).

1. Introduction

Circular economy relies on the extensive reuse of waste materials in the manufacturing of new articles. This is undoubtedly not straightforward for 'mixed' wastes, i.e. masses comprising materials of different nature and origin (metals, plastics, ceramics), as found in many landfills; however, the need for urban spaces from the remediation of landfills and for saving natural resources is pushing towards models of 'enhanced landfill mining' [1].

This paper is dedicated to a waste glass, belonging to the $CaO\text{-}Al_2O_3\text{-}Fe_2O_3\text{-}SiO_2$ system, from the plasma processing of municipal solid waste. Plasma heating is an effective technology for resource recovery from waste, since it provides both gasification of organics, by pyrolysis, and metal separation upon melting (owing to reducing conditions) [2]. The energy production from waste-derived gas ('Syngas') and the recovery of metals are undoubtedly profitable, but a true circular economy approach (and a truly 'enhanced' landfill mining) is realized only if also the vitreous by-product of the plasma heating process ('Plasmastone') is reused in new materials.

Significant examples of reuse are associated with the alkali activation of aqueous suspensions of Plasmastone powders [3,4]. In condition of 'strong' activation (high amounts of alkali hydroxides or alkali silicates added) [3], Plasmastone undergoes a substantial dissolution, followed by condensation ('polymerization') of the dissolution product. The obtained 'inorganic polymer' resembles the characteristics of the well-known geopolymers (produced by dissolution of alternative silicate and alumino-silicate materials), so that it could be considered a valid alternative to Portland cement, as inorganic binder.

* Corresponding author.
E-mail address: enrico.bernardo@unipd.it (E. Bernardo).

https://doi.org/10.1016/j.conbuildmat.2019.117265
0950-0618/© 2019 The Author(s). Published by Elsevier Ltd.
This is an open access article under the CC BY-NC-ND license (http://creativecommons.org/licenses/by-nc-nd/4.0/).

A 'weaker' alkali activation (e.g. using alkali hydroxides in low molarity) does not lead to products directly usable after processing at low temperature (close to room temperature), but configures a fundamental processing step in the manufacturing of highly porous glass-ceramics [4]. More precisely, suspensions of fine glass powders in alkaline aqueous solutions may exhibit a marked pseudo-plasticity, according to the formation of gels just at the surface of glass particles, by partial dissolution. While in inorganic polymers the hardening is due at least partially to the formation of a three-dimensional alumino-silicate hydrate network structure, glass suspensions are mostly stabilized by the formation and interlocking of calcium silicate hydrates (C–S–H) [4-6]. Air bubbles, incorporated by intensive mechanical stirring (with the help of surfactants), at high shear rates and low viscosity, remain 'frozen' in glass suspensions when the stirring stops, at low shear rate and high viscosity. A cellular structure, available at low temperature by simple drying of hardened suspensions, is later consolidated by viscous flow sintering.

The additional firing step is not an issue, considering the energy and cost savings (due to the weaker activation) and the possible application of highly porous glass-ceramic products. In fact, glass-ceramic foams may enter the market of thermally and acoustically insulating building materials, currently dominated, as a non-flammable alternative to polymeric foams, by glass foams [7]. Glass foams are manufactured by a quite complex process [7], based on gas evolution (from selected additives) in pyroplastic masses created by the viscous flow sintering of the starting glass powders. Weak alkali activation of glass suspensions, followed by mechanical foaming and sintering, in separating foaming and sintering, brings important advantages. Since foaming is already achieved at low temperature, the consolidation of soda-lime glass occurs at just 700 °C; in waste-derived glasses, like Plasmastone, the overlapping of sintering and crystallization is also an opportunity to increase the mechanical properties of the final products [4].

For waste-derived glasses, the absolute stabilization of pollutants is an essential requirement for safe products. The mixing with recycled glass is useful in 'diluting' the pollutant and improve the densification by viscous flow sintering [4]. However, previous experiences have already highlighted that Plasmastone could lead to chemically stable glass-ceramic foams, after firing in air at 800–1000 °C, only by addition of boro-alumino-silicate glass, recovered from discarded pharmaceutical vials [4,8]. The present paper will show that controlling the firing atmosphere enabled an enhanced stabilization, even operating with common soda-lime glass as additive, and an extension of functionalities. More precisely, low processing temperatures and nitrogen atmosphere had a synergistic effect on the precipitation of Fe-rich crystalline phases (particularly magnetite, Fe_3O_4), in turn leading to products exhibiting moderate electrical conductivity, high relative permittivity and remarkable electromagnetic shielding effectiveness.

2. Experimental procedure

Plasmastone was gently provided by Scanarc Plasma Technologies AB (Hofors, Sweden). Received in form of granules with a mean particle size of 2 mm, it was ground into fine powders, below 75 μm, by dry ball milling. Plasmastone was then mixed with soda-lime glass (SLG) powders (medium particle size equal to 30 μm, provided by SASIL SpA, Brusnengo, Biella, Italy) or boro-alumino-silicate glass (BSG) powders (<45 μm, from disposed and crushed pharmaceutical vials, provided by Nuova OMPI Piombino Dese, Padova, Italy). The composition of the starting materials is reported in Table 1 [4].

Foams were produced according to the alkali activation-gel casting procedure previously reported [4,8]. Plasmastone/glass powders were first introduced in an alkaline aqueous solution (2.5 M NaOH/KOH, ratio 1:1; solid content of 68 wt%), under mechanical stirring at 400 rpm, and left for 3 h, to achieve partial dissolution. Suspensions of Plasmastone/glass powders were then cast in closed polystyrene (PS) containers and placed at 75 °C, for 3 h. The suspensions were later added with 4 wt% Triton X-100 surfactant (polyoxyethylene octyl phenyl ether – $C_{14}H_{22}O(C_2H_4O)_n$, n = 9–10, Sigma-Aldrich, Gillingham, UK) and subjected to intensive mechanical stirring (at 2000 rpm). Finally, the resulting 'green' foams were left for 48 h at 40 °C, for complete drying, before being extracted from the PS containers.

Table 1
Chemical composition of the starting materials (wt%).

	Plasmastone	SLG	BSG
SiO_2	34.26–37.32	71.9	72
TiO_2	0.60–0.67	0.1	
Al_2O_3	12.82–14.79	1.2	7
Fe_2O_3	20.92–24.84	0.3	
MnO	0.11–0.15		
MgO	1.18–2.40	4	
CaO	22.97–23.20	7.5	1
Na_2O	0.26–1.10	14.3	6
K_2O	0.32–0.51	0.4	2
P_2O_5	0.03–0.18		
B_2O_3			12

Unlike in previous studies, the sintering treatment was applied at 800–1000 °C, using a heating rate of 10 °C/min and a holding time of 1 h, in flowing nitrogen atmosphere. The mineralogical analysis of the resulting glass-ceramics, once powdered, was conducted by means of X-ray diffraction (XRD) (Bruker D8 Advance, Karlsruhe, Germany), using CuKα radiation, 0.15418 nm, 40 kV–40 mA, 2θ = 10–70°, step size 0.05°, 2 s counting time. The phase identification was performed by means of the Match!® program package (Crystal Impact GbR, Bonn, Germany), supported by data from Powder Diffraction File (PDF)-2 database (International Centre for Diffraction Data, Newtown Square, PA, USA).

Large fired samples were cut into cubes with approximate dimensions of 10 mm × 10 mm × 10 mm. The geometrical density (ρ_{geom}) of these specimens was determined from the weight-to-volume ratio, using a calliper and a digital balance. The apparent density ($\rho_{apparent}$) and the true density (ρ_{true}) were later measured by means of a gas pycnometer (Micromeritics AccuPyc 1330, Norcross, GA), operating with He gas on whole specimens or on powders, respectively. The density values were used to compute the amounts of open and closed porosity. The compressive strength of foams was measured at room temperature, by means of an Instron 1121 UTM (Instron Danvers, MA) operating with a cross-head speed of 1 mm/min. Each data point represents the average value of 5 to 10 individual tests.

Morphological and microstructural characterizations were performed by means of optical stereomicroscopy (AxioCam ERc 5 s Microscope Camera, Carl Zeiss Microscopy, Thornwood, New York, USA).

Leaching tests on foams fired in nitrogen were performed based on Norm EN 12457-4 [9], as done for analogous foams fired in air [4,8], on samples broken into pieces smaller than 4 mm. The pieces were immersed in pure distilled water, in order to obtain a liquid to solid ratio of 10, and left for 24 h, under mechanical stirring. Suspensions were poured in a smaller flask and centrifuged in order to separate the solid material from the liquid, later analysed by means of inductively coupled plasma mass spectrometry (ICP-MS). The heavy metal content of the eluate was compared to the Austrian Recycling Building Materials Ordinance [10] and to the values acceptable at landfills for inert waste and non-hazardous waste [11].

The conductivity of the materials was evaluated on disc samples (about 50 mm diameter and 6 mm). As shown by Fig. 1a, upper and lower areas were first painted with a silver conductive paint (SCP) and then connected with electrical wires, by means of copper tape with conductive adhesive (3 M Copper Foil Tape 1181). The lateral surfaces were carefully masked, in order to form (almost flat) conductive layers just on top and bottom surfaces. The equivalent model of the electrical configuration used in the analysis is an inductance L, due to the thread connections, in series with a parallel between a resistance R and a capacitance C, due to the cylindrical sample put between parallel plates, as shown by Fig. 1b.

The DC value of R was measured by means of a Fluke 23 III multimeter. A GW INSTEK LCR-819 precision LCR meter (frequency range: 12 Hz – 100 kHz) and an Agilent 4285 precision LCR meter (frequency range: 75 kHz – 30 MHz) were used for AC measurements. The measured resistance R, given the geometry of the samples and according to Ohm's law, yielded an estimation of the electrical conductivity. The measured capacitance C, given the geometry and the parallel plates capacitor configuration, yielded an estimation the relative permittivity.

The shielding effectiveness (SE) in the frequency range 100 kHz – 3 GHz was measured with a different set-up: hollow cylindrical samples were placed in a coaxial holder with a continuous inner conductor, connected to a vector network analyser Agilent E5061B. This setup yielded the S_{21} parameter, in turn leading to the shielding effectiveness $SE_{dB} = - S_{21dB}$ [12–14].

3. Results and discussion

3.1. Microstructural analysis

The low temperature hardening of alkali-activated aqueous suspensions of Plasmastone powders relied on the formation of calcium silicate hydrate (C-S-H) compounds on the surface of each granule, as an effect of partial dissolution [4]. The addition of glass powders was intended to enhance the formation of C-S-H gel: this was effectively found for soda-lime glass, whereas boro-aluminosilicate glass could not contribute, due to the practical absence of CaO in the formulation [4]. In any case, very homogeneous foams could be obtained from both Plasmastone mixed with SLG (Fig. 2a) and BSG (Fig. 2b); the evident interconnections testify a mostly open porosity.

800 and 1000 °C were considered as the reference temperatures for the firing treatments, based on previous investigations [4,8]. 800 °C actually corresponds to the crystallization temperature of Plasmastone [4], so that viscous flow sintering was seriously impeded by the precipitation of crystals. The addition of soda-lime glass and the enhancement of firing temperature up to 1000 °C were expected to modify the viscous flow sintering/crystallization balance, with the softened glass additive, not prone to crystallization, offering extra liquid phase upon firing.

Fig. 3a shows that the glass addition could be significant even at 800 °C. The cellular structure remained substantially unaltered (with mostly open porosity), from the 'green' state, but with particles well 'glued' together. Firing at 1000 °C slightly increased the overall porosity, owing to gas evolution (from high temperature reduction of Fe^{3+} into Fe^{2+}: $2\ Fe_2O_3 \rightarrow 4\ FeO + O_2$ [15]), but there was no coarsening (see Fig. 3c).

The substantial equivalence between samples produced at different temperatures, in air, may be inferred from the porosity and strength data reported in Table 2. The strength of the solid phase (σ_{bend}) could be estimated from the measured crushing strength and density values, according to the Gibson & Ashby model [15] for open-celled foams (from the model, $\sigma_{comp} \sim 0.2 \cdot \sigma_{bend} \cdot (\rho_{rel})^{1.5} = 0.2 \cdot (\rho_{geom}/\rho_{true})^{1.5}$, so: $\sigma_{bend} \sim 5 \cdot \sigma_{comp} \cdot (\rho_{true}/\rho_{geom})^{1.5}$). Passing from 800 to 1000 °C the strength remained practically unaltered, on values consistent with those typically attributed to soda-lime glass (~70–75 MPa) [16].

Sintering in nitrogen led to quite surprising changes. At 800 °C (Fig. 3b) pores were visibly smaller; at 1000 °C (Fig. 3d) the pore size was similar to that of foams fired in air, at the same temperature. In all cases, the colour changed from brown-red to dark grey. The closed porosity (Table 2) did not increase; on the contrary, the porosity in samples fired in nitrogen remained open in all conditions. The cellular structure developed upon firing in nitrogen probably derived from a substantial 'reshaping' of pores, with contributions to porosity from overlapping phenomena, like the above-mentioned oxygen release, by reduction of Fe^{3+} into Fe^{2+}.

Firing in N_2 had a different impact on crushing strength: while the foams sintered at 1000 °C were stronger than those processed in air, at the same temperature, the foams sintered at 800 °C were weaker (the observed crushing strength is consistent with a bending strength of the solid phase of approximately 50 MPa). In any case, also the latter foams still compare favourably, in terms of strength-to-density ratio, with several commercial ceramic foams [17].

Fig. 4 testifies that increasing the firing temperature in air just enhanced the development of phases already present at 800 °C, such as hedenbergite ($Ca(Fe_{0.821}Al_{0.179})(SiAl_{0.822}Fe_{0.178})O_6$, PDF

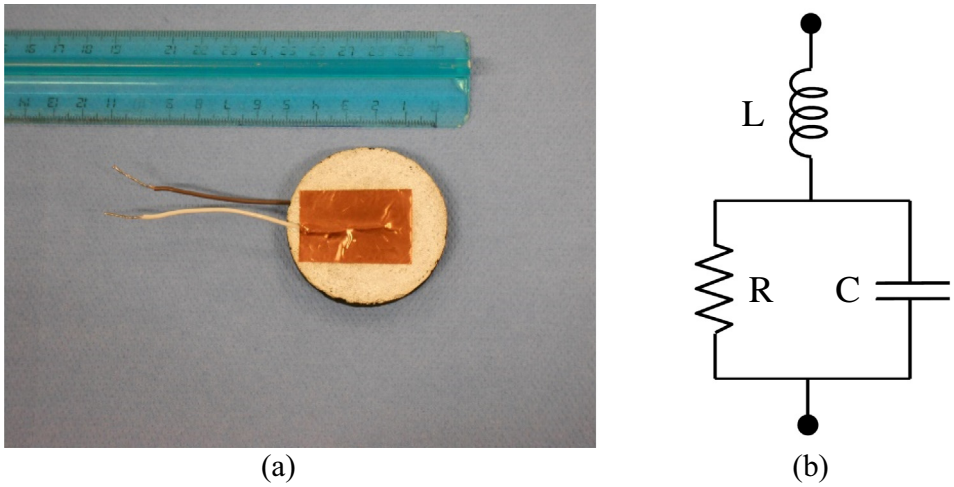

Fig. 1. Foamed sample coated with conductive paint and connected with threads: a) example; b) equivalent electrical model.

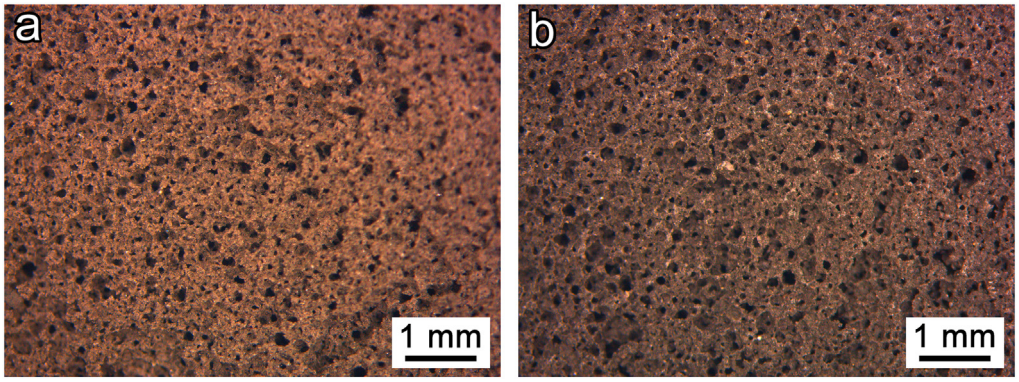

Fig. 2. Morphology of Plasmastone-derived samples (real colours) after low temperature hardening, from mixtures comprising recycled glasses: a) soda-lime glass; b) boro-alumino-silicate glass.

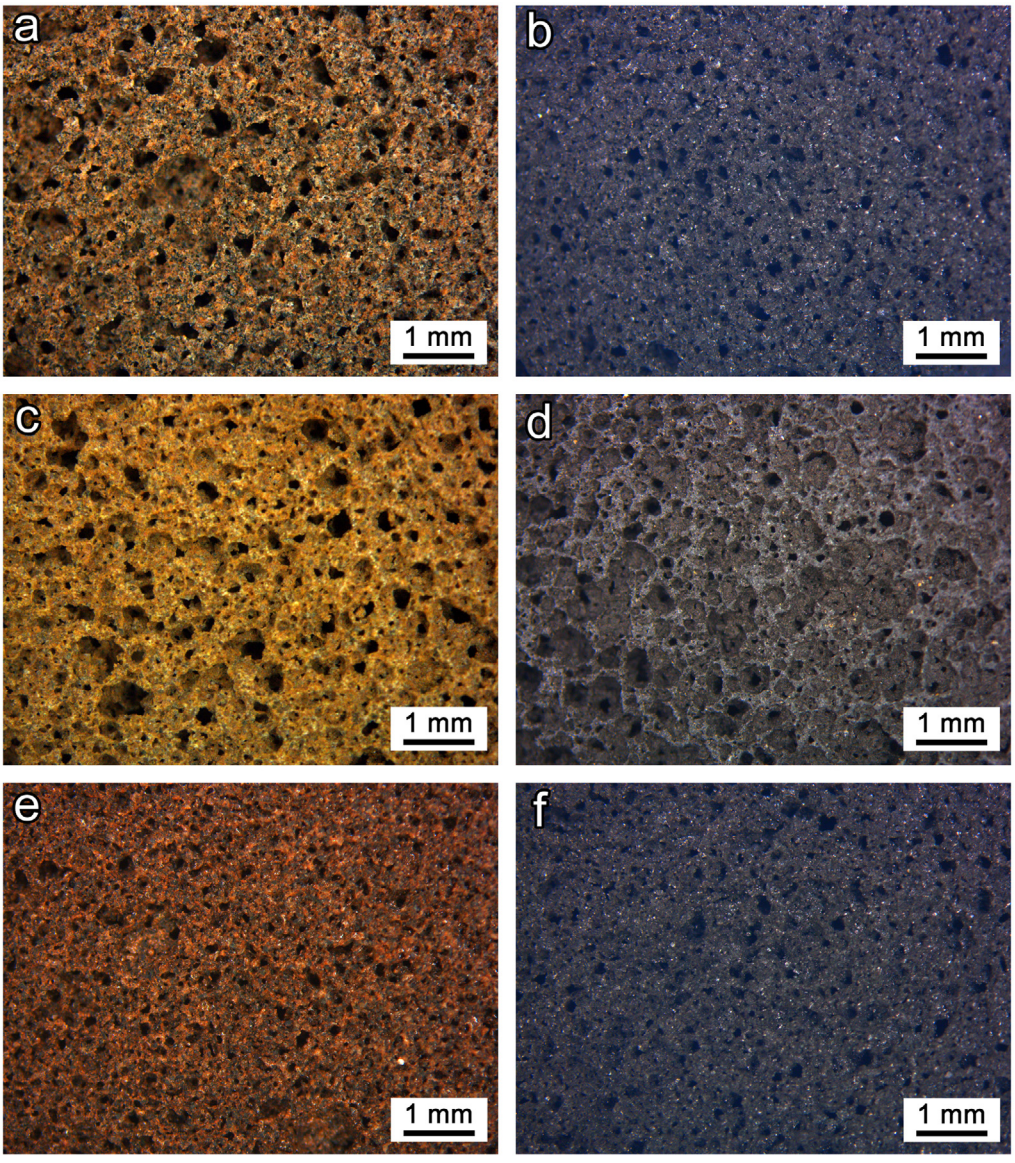

Fig. 3. Morphology of Plasmastone-derived samples after firing (real colours): SLG, 800 °C, in air (a) and in N_2 (b); SLG, 1000 °C, in air (c) and in N_2 (d); BSG, 800 °C, in air (e) and in N_2 (f).

#78-1546), andradite ($Ca_3Fe_2(SiO_4)_3$, PDF#84-1935) and wollastonite ($CaSiO_3$, PDF#84–0655). The firing at 1000 °C in N_2, on the contrary, favored the formation of Na-Mg-Fe doped gehlenite ($(Ca_{1.96}Na_{.05})(Mg_{.24}Al_{.64}Fe_{.12})(Si_{1.39}Al_{.61}O_7)$, PDF#72–2128), present

Table 2
Physical and mechanical properties of selected Plasmastone-based foams.

Glass additive	SLG				BSG	
Firing T (°C)	**800**		**1000**		**800**	
Atmosphere	Air [4]	**N_2**	Air [4]	**N_2**	Air [9]	**N_2**
ρ_{geom} (g/cm^3)	0.69 ± 0.01	0.78 ± 0.01	0.65 ± 0.02	0.77 ± 0.03	0.64 ± 0.04	0.74 ± 0.01
$\rho_{apparent}$ (g/cm^3)	2.74 ± 0.02	2.90 ± 0.10	2.92 ± 0.01	2.96 ± 0.01	2.24 ± 0.04	2.96 ± 0.02
ρ_{true} (g/cm^3)	2.90 ± 0.01	2.92 ± 0.01	3.20 ± 0.01	2.98 ± 0.01	2.71 ± 0.10	3.05 ± 0.01
Total porosity, P (%)	76.2	73.3	79.7	74.2	76.2	75.7
Open porosity, OP (%)	74.8	73.1	77.7	74.0	71.2	75.0
Closed porosity, CP (%)	1.4	0.2	2.0	0.2	5.0	0.7
Compressive strength, σ_{comp} (MPa)	1.7 ± 0.2	1.4 ± 0.4	1.4 ± 0.2	2.3 ± 0.4	2.0 ± 0.4	1.3 ± 0.6
σ_{bend} (MPa)	73.2	**50.7**	75.4	**87.6**	84.6	**54.4**

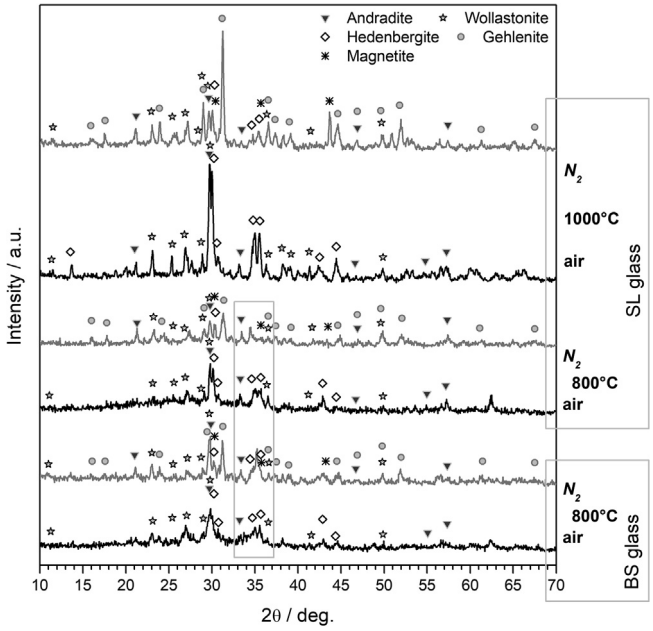

Fig. 4. Effect of temperature and firing atmosphere for samples from Plasmastone mixed with recycled glasses, SLG (SL) or BSG (BS).

in minor amounts at 800 °C. The presence of solid solutions of two groups, such as pyroxene (including hedenbergite) and melilite (including gehlenite), is quite typical for silicate glasses containing iron oxides [8,18,19]. The oxidation state of iron ions decreased, considering the reduction of andradite (featuring Fe^{3+}) and the increase of gehlenite, with the particular stoichiometry suggested by the phase identification software Match! (including Fe^{2+} ions). Some uncertainties, however, still derive from the fact that both pyroxene and melilite solid solutions may contain both Fe^{2+} and Fe^{3+} ions [20,21].

The phase assemblage was not significantly affected by the change of glass additive, passing from soda-lime glass to boro-alumino-silicate glass (Fig. 3e, f), with gehlenite traces appearing for the firing in nitrogen (Fig. 4). Also the crushing strength (Table 2) did not change substantially (at 800 °C, stronger foams in air, weaker in nitrogen).

The samples fired in nitrogen were subjected to a more detailed mineralogical analysis, especially concerning the peaks attributed to magnetite (Fe_3O_4, PDF#89-0691). The overlapping of peaks of iron oxide phases with the previously mentioned silicate phases, in fact, impeded a clear discussion, from Fig. 4 (especially in the 2θ range marked by the box). In Fig. 5 we report the patterns collected at 800 °C, in various conditions (glass additive, atmosphere) with the specific purpose of studying the contribution to the diffraction signals from iron oxide phases. Whereas the sample fired at 1000 °C, with soda-lime glass, exhibited peaks distinctively attributable to just to a single magnetite polymorph (e.g. the peaks for 2θ–43.5°), the samples fired at 800 °C featured additional contributions.

Besides the previously mentioned magnetite polymorph (labelled as 'M1′), we cannot exclude the presence of other two forms (labelled as 'M2′, PDF#89-0951, and 'M3′, PDF#89-6466). All forms have been recognized in the literature [22–24]. In addition, some peaks are compatible with hematite (Fe_2O_3, PDF#89-2810). The polymorphism of Fe_3O_4 is already known: the specific iron oxide exhibits many possible crystal structures passing from cubic inverse spinel to perovskite-based orthorhombic [25], with complications arising from the varying site occupancy [26]. M1 and M2 are attributable to a cubic symmetry (Fd-3 m space group, according to the PDF-2 records displayed in Match!), while M3 is orthorhombic (Pbcm space group).

The intensity of the peaks cannot be considered as proportional to the relative amounts, for the above-mentioned overlapping with the signals from silicate phases. In particular, for the sample with soda-lime glass addition fired at 800 °C (Fig. 5, bottom left), the main peak of magnetite 'M2′ at 2θ–30° overlaps with the more intense peak of pyroxene, known to form by epitaxial growth on magnetite nuclei [27]); other peaks (e.g. at 2θ–18°) are more visible in the analogous sample fired in nitrogen.

From the mineralogical analysis we may conclude that, in any case, the presence of several iron oxide phases provides an explanation for peaks, especially around 2θ–35°, not indexed in Fig. 4 (see box in the same figure), for samples fired in nitrogen at 800 °C. The formation of several polymorphs could be favored by interaction with the atmosphere: as an example, it is known that magnetite-like structures may be formed with Fe^{2+} and Fe^{3+} balanced by oxygen ions mixed with nitrogen ions, instead of simply by oxygen ions (iron oxynitride [28]). The incorporation of nitrogen as well as the possible replacement of Fe^{2+} and Fe^{3+} ions with other metal ions further complicates the analysis, since solid solutions determine displacements in the position of diffraction peaks.

3.2. Assessment of chemical stability

The previous investigation on Plasmastone [4] had evidenced that the chemical stability of foams from alkali activation of Plasmastone-SLG mixture, fired in air, was not optimized. In particular, the leaching of chromium, molybdenum and vanadium was far exceeding the limits from the Austrian Recycling Building Materials Ordinance. The same investigation established that the replacement of soda-lime glass with boro-alumino-silicate (BSG) could stabilize the foams, sintered at 1000 °C (leachates reported as 'benchmark' in Table 3 [4]). A more recent investigation showed that the leaching of glass-ceramic foams from Plasmastone coupled

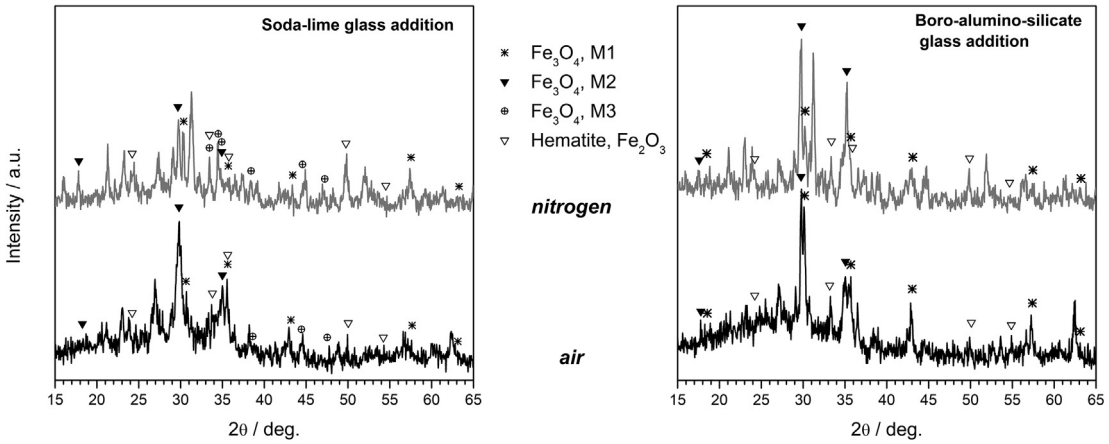

Fig. 5. Diffraction patterns of samples fired at 800 °C with indication of the overlapping with major peaks of iron oxide phases.

Table 3
Results of the leaching tests on porous materials fired in N_2.

	Limits Directive 2003/33/EC [12] (mg/kg)		Limits Austrian Recycling Building Materials Ordinance [11] (mg/kg)			Benchmark (mg/kg)	Observed leaching (mg/kg)		
Element	*Inert waste*	*Non-hazardous waste*	*U-A*	*U-B*	*D*	PS BSG 1000 °C air	PS BSG 800 °C N_2	PS SLG 800 °C N_2	PS SLG 1000 °C N_2
As	*0.5*	*2*				<0.0002	0.015	0.0135	0.0327
Ba	*20*	*100*			*20*	<0.0000	<0.0000	<0.0000	<0.0000
Cd	*0.04*	*1*			*0,04*	<0.0002	<0.0002	<0.0002	<0.0002
Cl			*800*	*1000*		–	–	–	–
Co					*1*	0.0012	<0.0012	<0.0012	<0.0012
Cr	*0.5*	*10*	*0.6*	*1*	*0.3*	0.0016	<0.0004	<0.0004	0.0062
Cu	*2*	*50*	*1*	*2*		0.0094	<0.0001	<0.0001	0.0113
F					*10*	–	–	–	–
Mo	*0.5*	*10*			*0.5*	0.0033	0.0322	0.3141	<0.0033
Ni	*0.4*	*10*	*0.4*	*0.6*		0.0014	<0.0014	<0.0014	0.0289
Pb	*0.5*	*10*				<0.0047	<0.0047	<0.0047	<0.0047
Sb	*0.06*	*0.7*				<0.0099	0.0314	0,0378	<0.0099
Se	*0.1*	*0.5*				<0.0122	0.0162	<0.0122	<0.0122
Tl					*0.1*	0.0064	<0.0064	<0.0064	<0.0064
V					*1*	0.0017	0.0048	0.0318	0.0063
W					*1.5*	–	–	–	–
Zn	*4*	*50*				<0.0203	<0.0203	<0.0203	<0.0203

with BSG were below the limits even after sintering, in air, at just 800 °C [8].

Table 3 shows that the leaching of all samples was lower than the limits for an inert material (class D). This finding is supported by the mineralogical changes, particularly by the formation of gehlenite instead of andradite, verified passing from SLG to BSG (in air) and, in general, from air to nitrogen as firing atmosphere (for both glass additives). In fact, it was already observed that an enhanced stabilization of heavy metals derives from reduced basicity (CaO/SiO_2 ratio) of the residual glassy phase [29], and gehlenite is effectively poorer, in silica content, than andradite.

3.3. Assessment of functionalities

Magnetite-containing composites already represent a valid solution for electromagnetic shielding [30]. A previous research actually evidenced some potential, in electromagnetic shielding, even for magnetite-containing porous waste-derived glass-ceramics [14], manufactured according to the same method here described.

A first hypothesis on the mechanism of electromagnetic shielding, based on electromagnetic losses in magnetization hysteresis, made with the previous investigations [4,8], must be revised. Magnetite is not only a ferri-magnetic material, but also an electronic conductor, owing to electron exchanges ('electron hopping') between iron sites possessing a different charge (Fe^{2+} and Fe^{3+}) [31,32]. Conductive materials are known to be good electromagnetic shields [33,34].

Samples fired in nitrogen atmosphere at 800 °C, as shown by Fig. 6a, b, exhibited a significant conductivity: the values are generally close to those of semiconductors [35].

From the measurements obtained on the two samples fired in nitrogen at 800 °C, done with precision LCR meters, we inferred an ohmic-inductive behaviour (negligible capacitance contribution in parallel with R). By using as model the series of L and R, the measured inductance was of the order of 100 nH, in agreement with the expected value associated with the connection threads from sample to LCR meter. From the experimental R data, we estimated the electrical conductivity (σ) from Ohm's law ($R = h/(\sigma \cdot A)$), with h and A height and area of top/bottom surface of disc samples).

The sample from PS/SLG mixture, fired in nitrogen atmosphere at 1000 °C, behaved differently, being ohmic-capacitive (parallel of R and C, with negligible contribution from the inductance of the threads). The conductivity was estimated from the measured resistance R, as done before. The relative permittivity (ε_r) was in turn estimated from the measured capacitance ($C = \varepsilon_0 \cdot \varepsilon_r \cdot A/h$, where ε_0

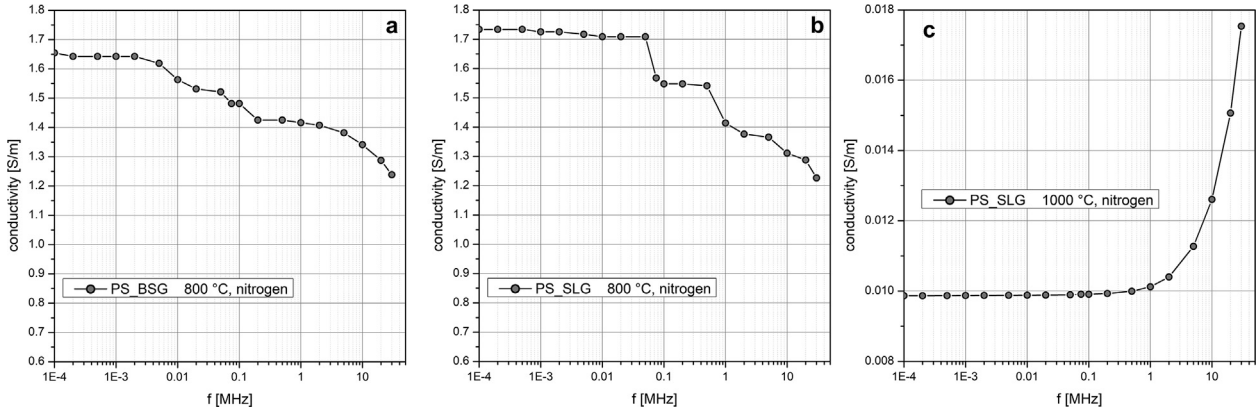

Fig. 6. Electrical conductivity of tested samples vs frequency.

is the vacuum permittivity). As shown by Fig. 6c, the conductivity values are about two order of magnitude lower than the ones obtained with the materials fired at 800 °C.

The data from RLC circuit were confirmed by DC resistance measurements, from which we inferred values of 2.1 S/m and 2.0 S/m for PS/BSG and PS/SLG samples, fired in nitrogen at 800 °C, respectively, and $9.8 \cdot 10^{-3}$ S/m for PS/SLG sample fired in nitrogen at 1000 °C.

Data reported in Fig. 7 show higher values of SE for the two materials with enhanced electrical conductivity. In Fig. 7a, the sample (with thickness of about 7 mm) from BSG addition exhibited a shielding effectiveness above 3 dB in all frequency range, with a peak value of about 10 dB near to 3 GHz. In Fig. 7b, the sample (with thickness of about 7 mm) from SLG addition had a lower value of SE than the previous case of about 1 – 2 dB in all frequency range, with a peak value of about 8 dB near to 3 GHz. On the other hand, the sample from SLG addition fired at 1000 °C (with thickness of about 8 mm), i.e. the material with the lowest electrical conductivity, had a very low value, at low frequencies, and a peak value of SE lower than 2.5 dB, as reported in Fig. 7c. As an estimation of the experimental error for the SE data, as reported in [13], the measurement system without sample and a central slit of 5 mm showed a negligible SE for frequencies less than 1.5 GHz and oscillations in the frequency range 1.5–3 GHz frequency range mostly below 1 dB.

A shielding effectiveness above 3 dB, also at low frequency, is significant, considering the results of other - even denser - waste-derived materials (with SE of about 3 dB for frequencies above 8 GHz) [36]. As mentioned above, shielding in an extended frequency range derived from the overlapping of electrical conductivity and 'magnetic' contributions. As pointed out by Chung [37], shielding effects due to conductivity are typically observed with a conductivity in the order of at least 0.01 S/m. Reflection losses, on the one hand, are present in all frequency range. In the case of an electrically conductive thin shield, absorption loss is about 0 dB; with an electrical conductivity not sensitive to frequency, reflection losses are known to derive simply by the product of thickness and the same electrical conductivity [33]. On the other hand, absorption losses increase with increasing frequency [37]. Therefore, for all the three samples analysed, at low frequency the found values of the SE, almost constant with frequency, are reasonably due to reflection losses, and some absorption due to the ferrimagnetisim of magnetite is the reason of the increase of SE found at high frequency.

Magnetite itself may be interpreted as the cause for electrical conductivity, but its role is conditioned by the available polymorphic variant: the poorly conductive sample, fired at 1000 °C, contained only one variant, whereas samples sintered at 800 °C featured two additional variants, as shown by Fig. 5. As evidenced by Blaney [38], the electrical conductivity is sensitive to metal deficiencies on octahedral sites (Fe^{2+} ions occupy one half of octahedral lattice sites, determined by the close packing of oxygen ions, whereas Fe^{3+} ions occupy the second half of octahedral sites and all tetrahedral lattice sites), in turn allowing for n- and p- type semiconductivity. A detailed structural investigation of magnetite polymorphic structures, with their impact on electrical properties, will constitute the focus of future efforts.

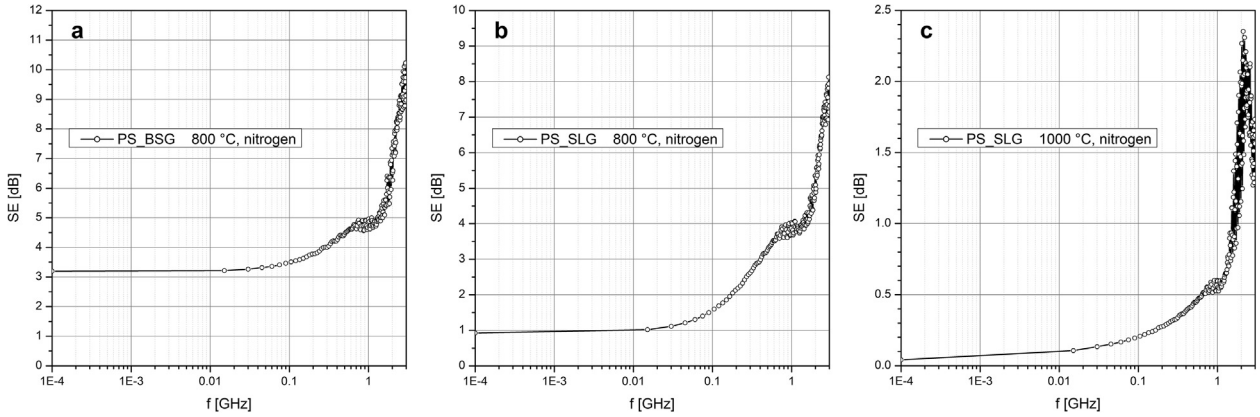

Fig. 7. Shielding effectiveness of tested samples.

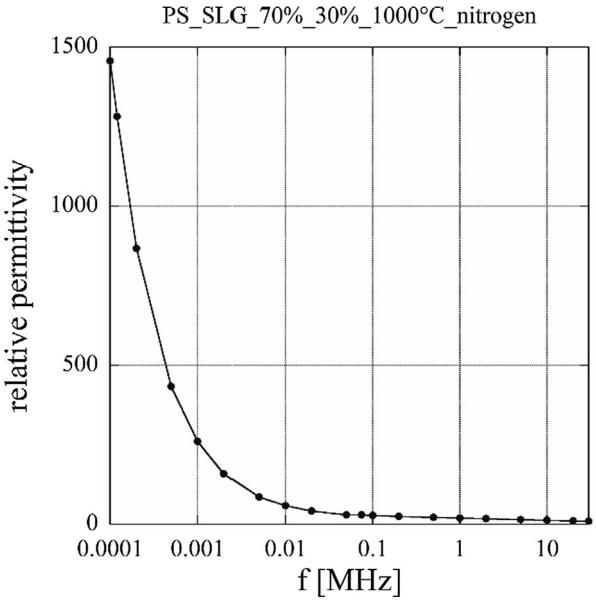

Fig. 8. Relative permittivity for PS/SLG 70 wt%/30 wt% fired in nitrogen atmosphere at 1000 °C.

The sample from SLG addition fired at 1000 °C, in nitrogen, could be interesting for other applications. Fig. 8 displays the measured values of relative permittivity, which exhibit a marked increase with decreasing frequency. Below 1 kHz the relative permittivity reached a particularly high level, approaching 1500 at 100 Hz. Huge permittivity values are known for magnetite and, generally, for complex iron-rich oxides with the same structure (ferrites) [39,40], and they are interpreted as an effect of interfacial polarization, in turn due to structural inhomogeneity and free charges, i.e. hopping electrons. The frequency sensitivity is attributed to the trapping of the hopping electrons operated by the same inhomogeneities [40], at low frequency. Higher frequencies 'unlock' the electron exchanges. Again, a detailed analysis of the particular crystal phase will constitute the focus of further investigations.

The present results are preliminary, but the shielding effectiveness of samples fired at 800 °C make them interesting as example of a new generation of safe, waste-derived materials that could minimize the human exposure to electromagnetic fields and reduce electromagnetic interferences. The sample fired at 1000 °C, with its particular dielectric characteristics, might be considered for novel electrical devices.

4. Conclusions

We may conclude that:

- Vitreous residues from the plasma processing of municipal solid waste may be upcyled in the manufacturing of glass-ceramic foams according to an alkali activation/foaming/sinter-crystallization process, with the support of soda-lime and pharmaceutical glass cullet; the firing in N_2 enabled the stabilization of pollutants operating with soda-lime glass addition, unlike in previous investigations (according to which, in air, only pharmaceutical glass could lead to stabilization);
- The enhanced stabilization, by firing in nitrogen, is interpreted as an effect of a different phase evolution, in turn enhancing the silica content in the residual glass phase;
- The firing in nitrogen favoured the separation of iron oxide as magnetite; at 800 °C magnetite was developed in several polymorphic variants;
- Treatments at 800 °C, in nitrogen atmosphere, led to electrically conductive glass–ceramic foams, exhibiting interesting electromagnetic shielding effectiveness values, in a vast frequency range with remarkable peaks at high frequency (about 8–10 dB with a material thickness of about 7 mm); this particular behaviour is likely due to overlapping contributions (electrical and magnetic);
- Besides electromagnetic shielding effectiveness, selected conditions (firing in nitrogen, soda-lime glass addition, sintering at 1000 °C) led to samples with particularly high relative permittivity (1500 at 100 Hz).

Declaration of Competing Interest

The authors declare that they have no known competing financial interests or personal relationships that could have appeared to influence the work reported in this paper.

Acknowledgements

The authors gratefully acknowledge the support of the European Community's Horizon 2020 Programme through Marie Skłodowska-Curie Innovative Training Networks "NEW-MINE" (Grant Agreement no. 721185, Patricia Rabelo Monich and Enrico Bernardo) and "CoACH-ETN", Grant Agreement no. 642557, Acacio Rincon Romero and Enrico Bernardo). Enrico Bernardo and Daniele Desideri acknowledge funding also from the Department of Industrial Engineering of the University of Padova, under the Twinning program 'MaVeRIF' ('Materiali Vetroceramici da Rifiuti Industriali per Applicazioni Funzionali' – E. Bernardo, D. Desideri).

References

[1] P.T. Jones, D. Geysen, Y. Tielemans, S. Van Passel, Y. Pontikes, B. Blanpain, et al., Enhanced Landfill Mining in view of multiple resource recovery: a critical review, J. Clean. Prod. 55 (2013) 45–55, https://doi.org/10.1016/j.jclepro.2012.05.021.
[2] Scanarc 2019. http://www.scanarc.se/ (accessed April 16, 2019).
[3] L. Machiels, L. Arnout, P. Yan, P.T. Jones, B. Blanpain, Y. Pontikes, Transforming enhanced landfill mining derived gasification/vitrification glass into low-carbon inorganic polymer binders and building products, J. Sustain. Metall. 3 (2017) 405–415, https://doi.org/10.1007/s40831-016-0105-1.
[4] P.R. Monich, A.R. Romero, D. Höllen, E. Bernardo, Porous glass-ceramics from alkali activation and sinter-crystallization of mixtures of waste glass and residues from plasma processing of municipal solid waste, J. Clean. Prod. 188 (2018) 871–878, https://doi.org/10.1016/j.jclepro.2018.03.167.
[5] I. Garcia-Lodeiro, E. Aparicio-Rebollo, A. Fernández-Jimenez, A. Palomo, Effect of calcium on the alkaline activation of aluminosilicate glass, Ceram. Int. 42 (2016) 7697–7707, https://doi.org/10.1016/j.ceramint.2016.01.184.
[6] M. Cyr, R. Idir, T. Poinot, Properties of inorganic polymer (geopolymer) mortars made of glass cullet, J. Mater. Sci. 47 (2012) 2782–2797, https://doi.org/10.1007/s10853-011-6107-2.
[7] R.D. Rawlings, J.P. Wu, A.R. Boccaccini, Glass-ceramics: their production from wastes – a review, J. Mat. Sci. 91 (2006) 733–761, https://doi.org/10.1007/s10853-006-6554-3.
[8] P.R. Monich, D. Desideri, E. Bernardo, Low temperature upcycling of vitreous byproduct of the MSW plasma processing into multifunctional porous glass-ceramics, Adv. Appl. Ceram. (2019) 1–6, https://doi.org/10.1080/17436753.2019.1595265.
[9] BSI, BS EN 12457-4:2002. Characterisation of waste. Leaching. Compliance test for leaching of granular waste materials and sludges, Quality. 3 (2002).
[10] RIS - Recycling-Baustoffverordnung (Austrian Recycling Building Materials Ordinance). https://www.ris.bka.gv.at/GeltendeFassung.wxe?Abfrage=Bundesnormen&Gesetzesnummer=20009212 (accessed April 11, 2019).
[11] Directive 2003/33/EC, 2003.
[12] A. Tamburrano, D. Desideri, A. Maschio, M. Sabrina Sarto, Coaxial waveguide methods for shielding effectiveness measurement of planar materials Up to 18 GHz, IEEE Trans. Electromagn. Compat. 56 (2014) 1386–1395, https://doi.org/10.1109/TEMC.2014.2329238.
[13] A. Maschio, E. Bernardo, D. Desideri, M. Marangoni, I. Ponsot, Y. Pontikes, Shielding effectiveness of construction materials, Int. J. Appl. Electromagn. Mech. 52 (2016) 137–144, https://doi.org/10.3233/JAE-162089.
[14] A. Rincón, D. Desideri, E. Bernardo, Functional glass-ceramic foams from 'inorganic gel casting' and sintering of glass/slag mixtures, J. Clean. Prod. 187 (2018) 250–256, https://doi.org/10.1016/j.jclepro.2018.03.065.

[15] L.J. Gibson, M.F. Ashby, Cellular solids: structure and properties, Cambridge University Press, Cambridge, UK, 1999.
[16] J.J. Mecholsky, R.W. Rice, S.W. Freiman, Prediction of Fracture Energy and Flaw Size in Glasses from Measurements of Mirror Size, J. Am. Ceram. Soc. 57 (1974) 440–443, https://doi.org/10.1111/j.1151-2916.1974.tb11377.x.
[17] CES EduPack 2018 materials education software. https://grantadesign.com/education/ces-edupack/.
[18] J. Williamson, J. Tipple, P.S. Rogers, Influence of iron oxides on kinetics of crystal growth in CaO-MgO-Al_2O_3-SiO_2 glasses, J. Iron Steel Inst. 206 (1968) 898–903.
[19] A.A. Francis, Non-isothermal crystallization kinetics of a blast furnace slag glass, J. Am. Ceram. Soc. 88 (2005) 1859–1863, https://doi.org/10.1111/j.1551-2916.2005.00354.x.
[20] G.J. Redhammer, Single-crystal X-ray diffraction and temperature dependent ^{57}Fe Mossbauer spectroscopy on the hedenbergite-aegirine (Ca, Na)(F^{e2+}, $^{Fe}3^{+}$)$_{s}i_2$O6 solid solution, Am. Mineral. 91 (2006) 1271–1292, https://doi.org/10.2138/am.2006.2173.
[21] V. Žáček, R. Skála, M. Chlupáčová, Z. Dvořák, Ca-Fe3+-rich, Si-undersaturated buchite from Zelenky, North-Bohemian Brown Coal Basin, Czech Republic, Eur. J. Mineral. 17 (2005) 623–634, https://doi.org/10.1127/0935-1221/2005/0017-0623.
[22] M. Marciello, V. Connord, S. Veintemillas-Verdaguer, M.A. Vergés, J. Carrey, M. Respaud, et al., Large scale production of biocompatible magnetite nanocrystals with high saturation magnetization values through green aqueous synthesis, J. Mater. Chem. B. 1 (2013) 5995–6004, https://doi.org/10.1039/c3tb20949k.
[23] S. Sundar, R. Mariappan, S. Piraman, Synthesis and characterization of amine modified magnetite nanoparticles as carriers of curcumin-anticancer drug, Powder Technol. 266 (2014) 321–328, https://doi.org/10.1016/j.powtec.2014.06.033.
[24] S. Bepari, N.C. Pradhan, A.K. Dalai, Selective production of hydrogen by steam reforming of glycerol over Ni/Fly ash catalyst, Catal. Today. 291 (2017) 36–46, https://doi.org/10.1016/j.cattod.2017.01.015.
[25] Y. Liu, Z.F. Gao, Q. Sun, Y.P. Zeng, The structure-tunable synthesis and magnetic properties of Fe3O4 nanocrystals, Hyperfine Interact. 219 (2013) 107–112, https://doi.org/10.1007/s10751-013-0811-z.
[26] M.E. Fleet, The structure of magnetite: defect structure II, Acta Crystallogr, Sect. B Struct. Crystallogr. Cryst. Chem. 38 (1982) 1718–1723, https://doi.org/10.1107/S056774088200702X.
[27] J. Feinberg, H.-R. Wenk, P. Renne, G. Scott, Epitaxial relationship of clinopyroxene-hosted magnetite determined using electron backscatter diffraction (EBSD) technique, J. Earth Planet. Mater. (2004), https://doi.org/10.2138/am-2004-2-328.
[28] F.C. Voogt, P.J.M. Smulders, G.H. Wijnja, L. Niesen, T. Fujii, M.A. James, et al., NO_2-assisted molecular-beam epitaxy of wustitelike and magnetitelike Fe oxynitride films on MgO(100), Phys. Rev. B. 63 (2002) 1–11, https://doi.org/10.1103/physrevb.63.125409.
[29] M. Romero, M.S. Hernández-Crespo, J.M. Rincón, Leaching behaviour of a glassy slag and derived glass ceramics from arc plasma vitrification of hospital wastes, Adv. Appl. Ceram. 108 (2008) 67–71, https://doi.org/10.1179/174367608x366337.
[30] G. Bantsis, C. Sikalidis, M. Betsiou, T. Yioultsis, T. Xenos, Electromagnetic absorption, reflection and interference shielding in X-band frequency range of low cost ceramic building bricks and sandwich type ceramic tiles using mill scale waste as an admixture, Ceram. Int. 37 (2011) 3535–3545, https://doi.org/10.1016/j.ceramint.2011.06.010.
[31] P. Lazor, O.N. Shebanova, H. Annersten, High-pressure study of stability of magnetite by thermodynamic analysis and synchrotron X-ray diffraction, J. Geophys. Res. Solid Earth. 109 (2004) 1–16, https://doi.org/10.1029/2003JB002600.
[32] W. Kündig, R. Steven Hargrove, Electron hopping in magnetite, Solid State Commun. (1969), https://doi.org/10.1016/0038-1098(69)90729-7.
[33] M.S. Sarto, A. Tamburrano, Innovative test method for the shielding effectiveness measurement of conductive thin films in a wide frequency range, IEEE Trans. Electromagn. Compat. 48 (2006) 331–341, https://doi.org/10.1109/TEMC.2006.874664.
[34] D.D.L. Chung, Electromagnetic interference shielding effectiveness of carbon materials, Carbon N. Y. 39 (2001) 279–285, https://doi.org/10.1016/S0008-6223(00)00184-6.
[35] M. Levinshtein, S. Rumyantsev, M. Shur, Handbook series on semiconductor parameters, World Sci., London (1996), https://doi.org/10.1142/2046-vol2.
[36] G. Bantsis, C. Sikalidis, M. Betsiou, T. Yioultsis, A. Bourliva, Ceramic building materials for electromagnetic interference shielding using metallurgical slags, Adv. Appl. Ceram. 110 (2011) 233–237, https://doi.org/10.1179/1743676111y.0000000009.
[37] D.D.L. Chung, Materials for electromagnetic interference shielding, J. Mater. Eng. Perform. 9 (2000) 350–354, https://doi.org/10.1361/105994900770346042.
[38] L. Blaney, Magnetite (Fe_3O_4): properties, synthesis, and applications, Lehigh Rev. 15 (2007). https://preserve.lehigh.edu/cas-lehighreview-vol-15/5.
[39] A. Radoń, D. Łukowiec, M. Kremzer, J. Mikuła, P. Włodarczyk, Electrical conduction mechanism and dielectric properties of spherical shaped Fe_3O_4 nanoparticles synthesized by co-precipitation method, Materials (Basel). 11 (2018), https://doi.org/10.3390/ma11050735.
[40] M.H. Abdullah, A.N. Yusoff, Complex impedance and dielectric properties of an Mg-Zn ferrite, J. Alloys Compd. 233 (1996) 129–135, https://doi.org/10.1016/0925-8388(96)80044-2.